JOURNAL OF CHEMICAL INFORMATION AND MODELING

Article

pubs.acs.org/jcim

Unraveling the Allosteric Inhibition Mechanism of PTP1B by Free Energy Calculation Based on Umbrella Sampling

Wei Cui,[†] Yuan-Hua Cheng,[‡] Ling-Ling Geng,[†] Den-Sheng Liang,[†] Ting-Jun Hou,*[,§] and Ming-Juan Ji*[,†]

[†]School of Chemistry and Chemical Engineering, University of Chinese Academy of Sciences, Beijing 100049, China

[‡]Department of Chemistry, Tsinghua University, 30# Shuangqing Road, Haidian District, Beijing 100084, P.R. China

[§]College of Pharmaceutical Sciences, Zhejiang University, Hangzhou, Zhejiang 310058, China

Supporting Information

ABSTRACT: Protein tyrosine phosphatase 1B (PTP1B) is a promising target for the treatment of obesity and type II diabetes. Allosteric inhibitors can stabilize an active conformation of PTP1B by hindering the conformational transition of the WPD loop of PTP1B from the open to the closed state. Here, the umbrella sampling molecular dynamics (MD) simulations were employed to compute the reaction path of the conformational transition of PTP1B, and the snapshots extracted from the MD trajectory were clustered into 58 conformational groups based on the key conformational parameter. Then, the impact of the conformational change of the WPD loop on the interactions between the allosteric site of PTP1B and an allosteric inhibitor BB3 was explored by using the MM/GBSA binding free energy calculations and free energy decomposition analysis. The simulation results show that the binding free energy of BB3 increases gradually from the open to the closed conformation of the WPD loop, providing the molecular mechanism of allosteric inhibition. Correlation analysis of the different energy terms indicates that the allosteric inhibitor with more negative van der Waals contribution cannot only exhibit stronger binding affinity but also hinder the swing of the WPD loop more effectively. Besides, it is found that the energy contribution of Lys292 in the α7 helix undergoes significant change, which reveals that Lys292 is not only the key residue for ligand binding but also plays an important role in hindering the conformational change of the WPD loop.

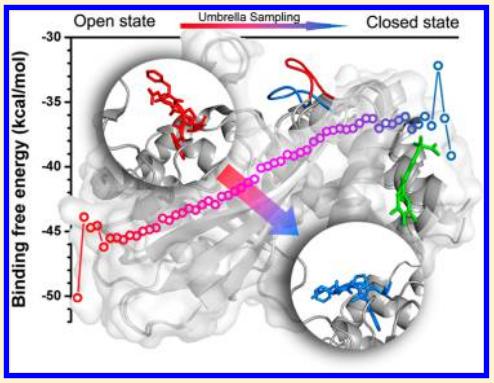

1. INTRODUCTION

Allosteric effect is one of the most common mechanisms in the regulation of catalytic activity of enzymes.[1−4] Protein tyrosine phosphatase 1B (PTP1B) regulates insulin signaling negatively by catalyzing the dephosphorylation reaction of phosphotyrosine substrates[5] and has become an important drug target for therapeutic intervention in type II diabetes,[6−8] obesity,[9] cancer, etc.[10,11] Full length PTP1B comprises 435 amino acids and has a canonical PTP domain with ∼280 residues in the N-terminal. PTP1B is regulated by the conformational change of the WPD loop (Trp179, Pro180, and Asp181),[12] a flexible loop closing to the binding pocket. The crystallographic studies show that the WPD loop of PTP1B exhibits an open or a closed state (Figure 1).[13−15] When the WPD loop opens, the binding pocket is easily accessible to substrate. Upon substrate binding, the WPD loop turns to the closed conformation to form a tight binding pocket.[16,17] Thus, the WPD loop is essential for the catalytic function of PTP1B.[18]

Because of the high conservation of the catalytic sites of protein tyrosine phosphatases (PTPs), the development of selective substrate-competitive inhibitors of PTP1B is quite challenging.[7] In 2004, Wiesmann et al. discovered a novel series of inhibitors with a benzofuran sulfonamide scaffold,[15] which show allosteric inhibition activity of PTP1B by preventing the closed conformation of the WPD loop. The allosteric binding site is ∼20 Å away from the catalytic site, and it is not well conserved and is substantially more hydrophobic than the binding active site. Thus, targeting the allosteric site provides an alternative strategy for developing selective inhibitors.[7] The allosteric site consists of several α helices, including the α3, α6, and α7 helices.[15] Crystal structures and equilibrium molecular

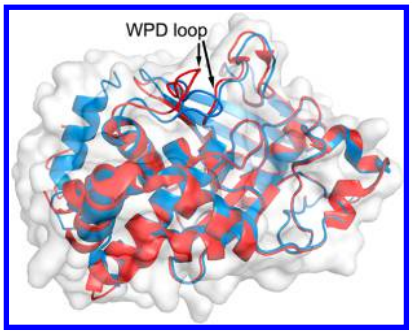

Figure 1. Comparison of the closed (blue) and open conformers (red) of the WPD loop in PTP1B. The structures were aligned by the coordinates of C_ω and the image was generated by Pymol 1.1.[13]

Received: November 1, 2012
Published: April 27, 2013

dynamics (MD) simulations can help us to elucidate the binding modes of allosteric inhibitors, but they cannot characterize the dynamic process of the large-scale conformational change upon inhibitor binding. Targeted molecular dynamics (TMD) simulations have been used to explore the conformational transition of the WPD loop of PTP1B.[12] However, the trajectory obtained from TMD usually leads to unphysical dynamics because incorrect transition states are often achieved.[19] In this study, a combination protocol based on umbrella sampling simulations,[20,21] MM/GBSA binding free energy calculations,[22−24] and binding free energy decomposition analysis[25−27] was employed to elucidate the allosteric inhibition mechanism of PTP1B.

2. MATERIALS AND METHODS

2.1. Preparation of Starting Conformation. The coordinates of the crystal structure of PTP1B with the open WPD loop in complex with the allosteric inhibitor BB3 (Scheme 1) were retrieved from Protein Data Bank (PDB entry: 1T48[15]). However, similar to most PTP1B structures with the open WPD loops, 1T48 does not have the coordinates of the α7 helix. In this study, 1T48 and a PTP1B structure with a closed WPD loop (PDB entry: 1PTV[14]) were aligned based on their backbone atoms between Glu1 to Gly283 except the WPD loop, and then the missing residues were extracted from 1PTV and merged into the structure of 1T48 using the SYBYL7.1 molecular simulation package.[28]

Scheme 1. 2D Structure of 3-(3,5-Dibromo-4-hydroxybenzoyl)-2-ethyl- benzofuran 6-Sulfonic Acid Dimethylamide (BB3)

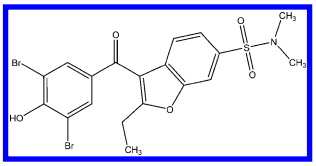

The inhibitor BB3 was optimized by Gaussian 03[29] at the HF/6-311G* level, and then the atomic partial charges were obtained by fitting the electrostatic potentials using the RESP fitting technique in Amber10.[30] The generations of the partial charges and the force field parameters for BB3 were accomplished using the *antechamber* program in AMBER10.[31]

In the molecular mechanics (MM) optimizations and MD simulations, AMBER03 force field,[32] and *gaff* force field[33] were used for PTP1B and BB3, respectively. The simulation was performed at pH 7.0, and the titratable residues, including lysine, arginine, aspartic acid, and glutamic acid, were typically charged, and the histidine residues were protonated at the epsilon position. The whole system was immersed with TIP3P water molecules[34] in a truncated octahedron box of 12 Å from any solute atoms. The system was neutralized with the counterions of Na^+. Prior to MD and umbrella sampling simulations, the system was minimized by the following three-stage protocol using the *sander* program in Amber10.[35] First, the protein was restrained, and solvent molecules and ions were relaxed (2000 cycles of steepest descent and 2000 cycles of conjugate gradient minimizations). Second, the protein backbone was restrained, and the side chains and the whole α7 helix were minimized (2500 cycles of steepest descent and 2500 cycles of conjugate gradient minimizations). Finally, the whole system was minimized without any restrain (2500 cycles of steepest descent and 2500 cycles of conjugate gradient minimizations).

2.2. MD and Umbrella Sampling Simulations. Before umbrella sampling, the initial structure was relaxed by 8 ns MD simulations in the canonical ensemble using the *pmemd* program in Amber10.[35] The system was gradually heated from 0 to 310 K over 60 ps. Then, 8 ns of canonical ensemble MD simulations were performed in a constant temperature of 310 K by the weak coupling algorithm.[36] SHAKE[37] was used to constrain bonds involving hydrogen atoms, and the time step was 2.0 fs. The particle mesh Ewald (PME) algorithm[38] was employed to calculate the long-range electrostatics. The nonbonded cutoff was set to 10 Å. During the sampling process, the coordinates were saved every 0.2 ps.

Then, the umbrella sampling MD simulations were carried out with the *sander* program in AMBER10 to simulate the conformational transition path of the WPD loop. During the simulations, a conformational parameter, the C_α-dihedral of Trp179,[39] was selected as the reaction coordinate of the reaction path for the conformational change of the PTP1B WPD loop. According to Kamerlin's study,[39] the C_α-dihedral of Trp179, which is a dihedral angle formed by the four C_α atoms of residues 178, 179, 180, and 181, was found to be one of the most important indicators for distinguishing the two different states of the WPD loop, and the C_α-dihedrals of Trp179 for the open and the closed states are around 247° and 211°, respectively. Here, the whole simulations consist of 37 simulation windows by steadily decreasing the C_α-dihedral of Trp179 from 247° to 211° with a step of 1°. For each sampling window, the C_α-dihedral of Trp179 was restrained to the new value by an artificial harmonic biasing potential with a force constraint of 50 kcal/mol rad^2. The MD simulations of 500 ps were performed for each sampling window, and a constant temperature of 310 K was controlled by the weak coupling algorithm. SHAKE was applied to fix all bonds involving hydrogen atoms, and the time step was 2.0 fs. The last snapshot of each sampling window was used as the starting coordinates for the next sampling window, and the conformation of the PTP1B−BB3 complex was transformed from the WPD loop open state to the closed state step by step in the conformational space. The coordinates and the value of the Trp179 C_α-dihedral were recorded every 1 ps. For each sampling window, the first 100 ps was discarded as the equilibration period, and 400 snapshots were extracted from the last 400 ps trajectory uniformly. Thus, from the whole umbrella sampling simulations, 14,800 snapshots were picked out totally. In order to compare the conformational change of the WPD loop, the MD simulations were performed for the PTP1B without BB3. The fixed 1T48 structure was used as the initial structure, and the inhibitor was removed. The whole protein was solvated and relaxed. Finally, the umbrella sampling MD simulations were carried out based on the same protocol for the PTP1B−inhibitor complex.

2.3. Binding Free Energy Prediction and Energy Decomposition. On the basis of the values of the Trp179 C_α-dihedrals, all the 14,800 snapshots were clustered into different conformation groups, and the Trp179 C_α-dihedrals for all conformations in the same conformation group differ by less than 1°. In total, 58 conformation groups were obtained after removing these conformation groups with less than 20 snapshots. Then, the binding free energies of BB3 for 58 conformation groups were calculated using the MM/GBSA technique according to the following equation.[40−54]

$$\begin{aligned}\Delta G_{\text{binding}} &= G_{\text{complex}} - G_{\text{protein}} - G_{\text{ligand}} \\ &= \Delta H + \Delta G_{\text{solvation}} - T\Delta S \\ &= \Delta E_{\text{MM}} + \Delta G_{\text{GB}} + \Delta G_{\text{SA}} - T\Delta S \end{aligned} \quad (1)$$

where ΔE_{MM} is the gas-phase interaction energy between protein and ligand, including the electrostatic (ΔE_{ele}) and van der Waals (ΔE_{vdw}) contributions; ΔG_{GB} and ΔG_{SA} are the polar (electrostatic) and nonpolar contributions to desolvation upon ligand binding, respectively; and $T\Delta S$ is the conformational entropy at temperature T. Here, the electrostatic desolvation free energy was calculated by the Generalized Born (GB) model developed by Tsui and Case.[55] The PTP1B−inhibitor binding interface is relatively hydrophobic, and therefore, the solvent and the solute dielectric constants of GB were set to 80 and 1, respectively.[45] The nonpolar desolvation term was estimated from the solvent accessible surface area (SASA): $G_{\text{np}} = 0.0072 \times \text{SASA} + 0.00$.[56] The calculations of the binding free energy were accomplished with the *mm_pbsa.pl* program in AMBER10. Because of the high computational demand and low prediction accuracy, we only calculated the conformational entropies of the 247° and 211° groups to evaluate the trend of the entropy change during the conformational change. We picked out eight snapshots uniformly form each group, and the *nmode* program in AMBER10 was used to compute the conformational entropy.

The total binding free energy of BB3 for each conformation group was decomposed into inhibitor−residue pairs using the MM/GBSA decomposition analysis by the *mm_pbsa* program in AMBER10.[25−27,57−59] The energy contribution for each inhibito−residue pair has four parts: van der Waals term (ΔE_{vdw}), electrostatic term (ΔE_{ele}), polar desolvation term (ΔG_{GB}), and nonpolar desolvation term (ΔG_{SA}). The polar desolvation term was calculated by the GB model developed by Tsui and Case, and the nonpolar desolvation term was estimated from the surface area with the LCPO model.

3. RESULTS AND DISCUSSION

3.1. Conformational Analysis. Figure 2 shows a smooth decline of the C_α-dihedral of Trp179 throughout the entire simulations, indicating that this important conformational parameter varies smoothly by imposing the harmonic biasing potential. In Kamerlin's study,[39] they used five parameters to monitor the conformational change of the WPD loop, and these five parameters include the distance between C_α of Phe182 and C_α of Gly218 that changes from 17.51 Å in the open state (PDB entry: 1T48) to 12.52 Å in the closed state (PDB entry: 1PTV), the distance between O of Trp179 and N_η of Gly218 that varies from 5.60 to 2.90 Å, the C_α-dihedral of Gly183 from −66.42° to −100.92°, the C_α-dihedral of Phe182 from −11.01° to 78.78°, and the C_α-dihedral of Trp179 from −114.66°(~247°) to −159.75°(~211°). According to Kamerlin's study,[39] the Trp179 dihedral angle is a better conformational descriptor to characterize the conformational transition of the WPD loop than the Gly183 and Phe182 dihedral angles. Certainly, the swing of the WPD loop is not a simple motion, and these conformational descriptors should be closely correlated during the loop closing (opening).

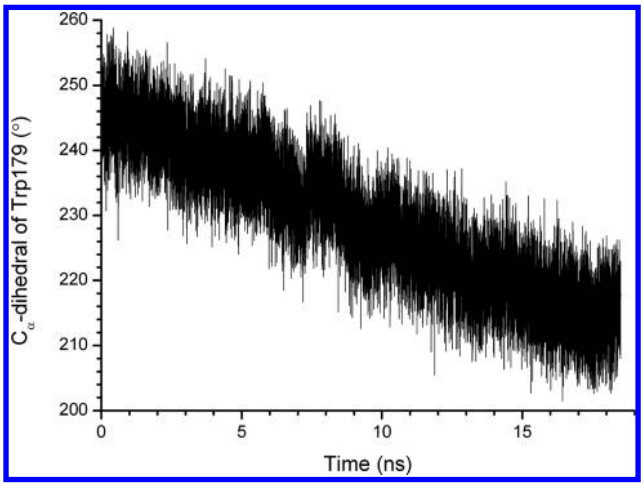

Figure 2. Time evolution of the C_α-dihedral of Trp179 from the umbrella sampling simulations.

Here, besides the C_α-dihedral of Trp179, the other four important conformational parameters studied by Kamerlin et al. were also analyzed and compared with the C_α-dihedral of Trp179. All the five parameters demonstrate obvious difference between the open and the closed states of the WPD loop, and the C_α-dihedral of Trp179 versus each of the other four parameters shows non-centrosymmetric distribution in scatter diagram (Figure S1, Supporting Information). Considering that the high complexity of the collective motion of the WPD loop, it is impossible to obtain perfect linear relationships between these conformational parameters. However, the non-centrosymmetric distributed scatter diagrams (Figure S1, Supporting Information) suggest that the changes of the four conformational parameters are in accordance with the change of the C_α-dihedral of Trp179. Because the C_α-dihedral of Trp179 changes smoothly, it is obvious to infer that the conformation of the WPD loop changes smoothly during the umbrella sampling simulations. Therefore, it is reasonable to analyze the profile of the binding affinity of the allosteric inhibitor during the conformational transition of the WPD loop of PTP1B by binding free energy calculations.

3.2. Binding Free Energy Profile of BB3. In order to obtain the binding free energy profile of the allosteric inhibitor BB3 during the conformational transition of the WPD loop, MM/GBSA was used to calculate the binding free energy of BB3 for the conformation groups obtained from the clustering of the snapshots extracted from the umbrella sampling MD trajectory. Results of the MM/GBSA calculations for all 58 conformation groups are summarized in Table 1. As shown in Table 1, the binding free energy of the typical open WPD loop conformation group with the Trp179 C_α-dihedral of 247° is −44.98 kcal/mol, while that of the typical closed WPD loop conformation group with the Trp179 C_α-dihedral of 211° is −37.03 kcal/mol. That is to say, the complex of PTP1B with the open WPD loop is 7.95 kcal/mol more stable than that with the closed WPD loop. Moreover, it is observed that the binding free energy increases gradually from the open conformation group to the closed conformation group, which indicates that the complex of PTP1B and BB3 becomes more unstable when the WPD loop changes from the open to the closed state.

The predicted conformational entropies show that the $T\Delta S$ of the 247° and 211° groups are −21.16 and −17.09 kcal/mol, respectively, suggesting that the inhibitor and its binding pocket become more flexible when the WPD loop swings from the open to closed state.

According to the energy terms of the binding free energies shown in Table 1, the major favorable contributor to inhibitor

Table 1. MM/GBSA Binding Free Energies of the Conformation Groups

C_α-dihedral of Trp179 (deg)	ΔE_{vdw} (kal/mol)	ΔE_{ele} (kal/mol)	ΔG_{GB} (kal/mol)	ΔG_{SA} (kal/mol)	ΔG_{tot} (kal/mol)
200	−48.93 ± 3.15	−8.08 ± 3.93	23.14 ± 4.18	−5.28 ± 0.31	−39.15 ± 2.26
201	−44.79 ± 2.73	−5.14 ± 3.97	19.21 ± 2.94	−5.54 ± 0.22	−36.26 ± 1.30
202	−41.93 ± 3.37	−5.08 ± 4.50	20.27 ± 3.86	−5.44 ± 0.21	−32.18 ± 1.99
203	−46.70 ± 4.37	−2.50 ± 4.55	17.78 ± 1.71	−5.44 ± 0.20	−36.83 ± 1.72
204	−45.51 ± 1.25	−5.71 ± 2.77	20.64 ± 3.49	−5.51 ± 0.14	−36.10 ± 1.21
205	−46.79 ± 2.26	−4.50 ± 3.06	20.16 ± 3.12	−5.58 ± 0.16	−36.72 ± 1.37
206	−46.12 ± 1.72	−6.76 ± 3.48	21.20 ± 3.18	−5.42 ± 0.09	−37.10 ± 1.66
207	−46.22 ± 1.92	−5.01 ± 3.80	20.57 ± 3.14	−5.47 ± 0.19	−36.13 ± 1.75
208	−46.61 ± 2.05	−6.65 ± 3.15	22.38 ± 2.63	−5.51 ± 0.16	−36.39 ± 1.56
209	−46.97 ± 1.77	−4.84 ± 3.64	20.65 ± 3.46	−5.53 ± 0.16	−36.68 ± 1.38
210	−46.96 ± 2.34	−5.66 ± 3.71	21.55 ± 3.38	−5.57 ± 0.16	−36.63 ± 2.00
211	−47.67 ± 2.01	−5.66 ± 3.85	21.89 ± 3.48	−5.60 ± 0.14	−37.03 ± 1.69
212	−46.79 ± 2.10	−4.42 ± 4.11	20.48 ± 3.61	−5.55 ± 0.17	−36.28 ± 1.70
213	−46.77 ± 1.90	−5.03 ± 3.75	21.11 ± 3.35	−5.58 ± 0.17	−36.26 ± 1.51
214	−47.45 ± 2.20	−4.64 ± 4.06	21.06 ± 3.68	−5.61 ± 0.14	−36.64 ± 1.87
215	−47.77 ± 2.17	−5.53 ± 4.08	21.85 ± 3.71	−5.59 ± 0.15	−37.03 ± 1.97
216	−47.66 ± 2.21	−5.37 ± 4.17	21.53 ± 3.79	−5.62 ± 0.18	−37.12 ± 1.79
217	−47.72 ± 2.27	−5.48 ± 4.42	21.79 ± 4.07	−5.63 ± 0.15	−37.04 ± 1.93
218	−47.94 ± 2.30	−6.02 ± 4.13	22.39 ± 3.66	−5.62 ± 0.18	−37.18 ± 2.05
219	−47.91 ± 2.39	−6.73 ± 4.17	22.99 ± 3.82	−5.62 ± 0.16	−37.27 ± 2.12
220	−48.61 ± 2.42	−6.66 ± 3.97	23.15 ± 3.65	−5.65 ± 0.16	−37.77 ± 2.17
221	−48.92 ± 2.40	−7.40 ± 3.95	23.89 ± 3.66	−5.64 ± 0.16	−38.06 ± 2.21
222	−49.43 ± 2.65	−8.19 ± 3.78	24.57 ± 3.45	−5.65 ± 0.16	−38.69 ± 2.34
223	−49.62 ± 2.47	−8.58 ± 3.65	24.96 ± 3.28	−5.65 ± 0.16	−38.89 ± 2.19
224	−49.89 ± 2.52	−8.73 ± 3.43	25.13 ± 3.16	−5.67 ± 0.18	−39.16 ± 2.18
225	−49.94 ± 2.64	−8.51 ± 3.55	25.07 ± 3.25	−5.68 ± 0.18	−39.06 ± 2.31
226	−50.41 ± 2.84	−8.51 ± 3.20	25.03 ± 2.87	−5.69 ± 0.19	−39.57 ± 2.33
227	−50.63 ± 2.99	−8.87 ± 3.38	25.48 ± 3.05	−5.70 ± 0.18	−39.72 ± 2.41
228	−51.00 ± 2.88	−8.69 ± 3.33	25.43 ± 2.91	−5.70 ± 0.20	−39.96 ± 2.28
229	−51.21 ± 3.01	−8.10 ± 3.27	24.93 ± 2.82	−5.72 ± 0.18	−40.10 ± 2.58
230	−52.38 ± 2.96	−7.38 ± 3.38	24.58 ± 2.87	−5.77 ± 0.18	−40.96 ± 2.47
231	−52.79 ± 3.04	−7.06 ± 3.68	24.43 ± 3.13	−5.80 ± 0.19	−41.22 ± 2.45
232	−53.40 ± 2.86	−6.40 ± 3.82	24.04 ± 3.34	−5.86 ± 0.18	−41.62 ± 2.26
233	−53.67 ± 2.82	−6.54 ± 3.75	24.18 ± 3.15	−5.86 ± 0.18	−41.90 ± 2.36
234	−54.23 ± 2.73	−5.25 ± 3.79	23.19 ± 3.24	−5.92 ± 0.18	−42.21 ± 2.23
235	−54.43 ± 2.69	−4.96 ± 3.79	23.01 ± 3.31	−5.94 ± 0.17	−42.31 ± 2.30
236	−55.39 ± 2.75	−4.16 ± 3.73	22.61 ± 3.30	−5.98 ± 0.16	−42.92 ± 2.44
237	−55.07 ± 2.79	−4.15 ± 3.98	22.57 ± 3.41	−5.98 ± 0.17	−42.64 ± 2.51
238	−55.46 ± 2.77	−3.56 ± 4.00	22.11 ± 3.49	−6.01 ± 0.15	−42.93 ± 2.56
239	−55.83 ± 2.76	−3.37 ± 3.96	21.87 ± 3.42	−6.02 ± 0.16	−43.35 ± 2.45
240	−55.77 ± 2.82	−2.99 ± 4.03	21.57 ± 3.51	−6.04 ± 0.15	−43.22 ± 2.60
241	−56.23 ± 2.81	−2.74 ± 3.90	21.47 ± 3.50	−6.06 ± 0.13	−43.56 ± 2.64
242	−56.21 ± 2.81	−3.23 ± 4.19	21.79 ± 3.71	−6.08 ± 0.14	−43.73 ± 2.62
243	−56.59 ± 2.60	−3.18 ± 3.99	21.72 ± 3.45	−6.10 ± 0.12	−44.14 ± 2.66
244	−56.50 ± 2.80	−3.04 ± 3.89	21.66 ± 3.44	−6.11 ± 0.13	−43.98 ± 2.73
245	−57.09 ± 2.83	−3.83 ± 4.22	22.32 ± 3.59	−6.11 ± 0.11	−44.72 ± 2.80
246	−57.28 ± 2.66	−3.76 ± 4.24	22.29 ± 3.30	−6.10 ± 0.12	−44.85 ± 2.63
247	−57.46 ± 2.47	−3.68 ± 4.31	22.26 ± 3.74	−6.10 ± 0.13	−44.98 ± 2.49
248	−57.43 ± 2.45	−5.42 ± 3.92	23.62 ± 3.16	−6.12 ± 0.09	−45.35 ± 2.62
249	−57.84 ± 2.73	−4.20 ± 4.15	22.86 ± 3.71	−6.12 ± 0.10	−45.29 ± 2.59
250	−57.82 ± 2.32	−5.35 ± 4.01	23.62 ± 3.44	−6.11 ± 0.11	−45.65 ± 2.26
251	−58.25 ± 2.02	−5.07 ± 3.83	23.94 ± 3.21	−6.10 ± 0.12	−45.48 ± 2.40
252	−58.04 ± 2.21	−4.41 ± 5.06	23.07 ± 3.73	−6.13 ± 0.09	−45.52 ± 2.70
253	−58.06 ± 1.25	−7.31 ± 5.04	25.30 ± 3.50	−6.14 ± 0.11	−46.20 ± 1.92
254	−57.00 ± 2.37	−4.10 ± 4.34	22.70 ± 4.13	−6.15 ± 0.15	−44.55 ± 2.59
255	−56.56 ± 2.11	−9.17 ± 4.01	27.25 ± 2.80	−6.23 ± 0.12	−44.71 ± 2.05
256	−59.11 ± 1.89	0.04 ± 3.86	21.21 ± 4.28	−6.02 ± 0.09	−43.89 ± 1.45
257	−61.80 ± 1.30	−11.3 ± 4.43	29.08 ± 3.13	−6.12 ± 0.10	−50.14 ± 1.63

dx.doi.org/10.1021/ci300526u | J. Chem. Inf. Model. 2013, 53, 1157−1167

binding is the van der Waals term. Then, we compared the correlations between the predicted binding free energies and each energy term (Table 1). We found that the nonpolar contribution ($\Delta E_{vdw} + \Delta G_{SA}$) has linear correlation ($r = 0.66$) with the total binding free energy, while the polar contribution ($\Delta E_{ele} + \Delta G_{GB}$) has anti-linear correlation ($r = -0.19$) with the binding free energy. The Z-test shows that the correlation between the nonpolar contribution and total binding free energy is statistically significant (Part1, Supporting Information). Moreover, the Hotelling's *t*-test for those two correlation coefficients shows that the correlation coefficient of the nonpolar contribution and total energy is significant higher than that of the polar contribution and total energy, suggesting that the nonpolar contribution, especially the van der Waals term, determines the difference of the binding affinities of BB3 in different conformation groups. Therefore, according to the correlation analysis, it can be inferred that the nonpolar interactions ($\Delta E_{vdw} + \Delta G_{SA}$) play an important role in the allosteric inhibition of the conformational transition of the WPD loop.

Compared with the electrostatic interactions, the van der Waals interactions between PTP1B and BB3 are more sensitive to the conformational transitions. In this complex, the binding site of BB3 is composed of the α3, α6, and α7 helices. The WPD loop and the α3 helix are neighboring in the primary structure of PTP1B, and then it is reasonable that the allosteric binding site varies with the movement of the WPD loop, and the van der Waals interactions between PTP1B and BB3 change accordingly. Therefore, along with the increase of the van der Waals interactions during the umbrella sampling simulations, the complex of PTP1B and BB3 becomes more unstable.

In order to analyze the variation rate of the binding free energies with the change of the C_α-dihedral of Trp179, the differences of the total binding free energy and each energy term were obtained by subtracting the energy values of two neighboring conformation groups. Most of the differences of the total binding free energies are negative, which is consistent with the aforementioned inference that the complex of PTP1B with BB3 becomes more unstable with the closing of the WPD loop.

In summary, the correlation analyses of the binding free energy terms and their differences show the PTP1B–BB3 complex becomes more unstable when the WPD loop changes from the open to the closed state. The van der Waals interactions play a crucial role in the stability of the complex. According to the above discussions, we believe that an allosteric inhibitor with more favorable van der Waals contribution not only has higher binding affinity but also can hinder the swing of WPD loop more efficiently. In contrast, an allosteric inhibitor with more favorable electrostatic contribution may also has better binding affinity, but due to the anticorrelation between the polar term and the total binding energy, it is impossible for the electrostatics-dominant inhibitor to be as effective as the inhibitor with more favorable van der Waals contribution to control the movement of the WPD loop.

3.3. PTP1B-BB3 Interaction Spectra. To analyze the energy contribution of each residue in the allosteric site, the MM/GBSA free energy decomposition analysis was conducted for all conformation groups. Figure 3 shows the PTP1B–BB3 interaction spectra for the 211° and 247° conformation groups, which are the conformation groups with the typical closed and open states of the WPD loop. From Figure 3, it is clear that all

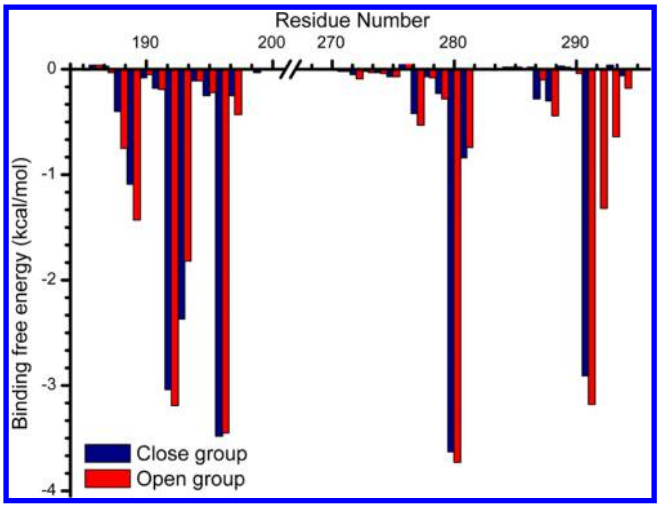

Figure 3. Residue–BB3 interaction spectra for (A) open and (B) closed conformation groups.

the residues with important contributions are located in the α3, α6, α7 helices distributed from the sequence 150–298. Furthermore, the important residues in the typical open and closed WPD loop groups are almost identical, but the energy contributions of the important residues in the typical open WPD loop group are generally more negative than those of the corresponding residues in the typical closed WPD loop groups.

For the purpose of revealing the relationship between each energy contribution of the important residues mentioned above, the correlations between the residues with respect to the total energy terms (ΔG_{tot}) and with respect to the nonpolar contributions ($\Delta E_{vdw} + \Delta G_{SA}$) were analyzed for the conformation groups, and the correlation coefficient matrices are visualized in Figure 4 using the Scilab software package.[60] The correlation matrix between all residues with respect to the total binding free energies is displayed in the top left corner of Figure 4A, while that with respect to the nonpolar contributions are in the lower right corner. Obviously, Figure 4A shows an approximately axial symmetry distribution relative to its diagonal. The symmetry in Figure 4A confirms that the nonpolar term is the main contributor to the total binding free energy. Moreover, the dark red or dark blue blocks around the diagonal indicate that the closely correlated residue–residue pairs may share similar movement patterns with neighboring residues, and according to the dark blocks, the key residues can be clustered into three groups, which are located in the α3, α6, and α7 helices, respectively.

The correlation maps for three pairs of regions are shown in Figure 4B–D. As shown in Figure 4B, the total energies between the residues in α6 and those in α7 are closely correlated, indicating that the two secondary structures share very similar movement patterns in the umbrella sampling simulations. The correlations between the total energies of the residues in α3 and those in α6–7 shown in Figure 4C have periodic patterns along the axis of the α3 residues, indicating that some residues in one side of the α3 helix share similar movement patterns with some residues in the α6 and α7 helices. In a word, these three secondary structures and the inhibitor can form a tight interaction network. The forced movement of the WPD loop leads to the mobility of the α3 helix, which further induces the instability of the whole α3, α6, and α7 interaction network and eventually disfavors the stable binding of the inhibitor to the allosteric site. The key residues

dx.doi.org/10.1021/ci300526u | J. Chem. Inf. Model. 2013, 53, 1157–1167

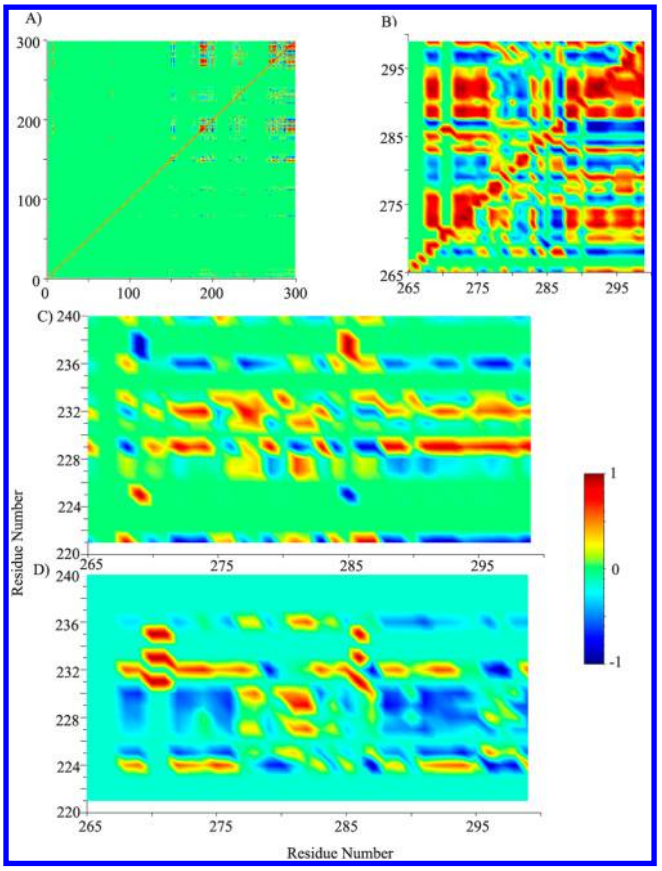

Figure 4. Visualization of the correlation coefficient matrix for each residue−residue pair based on (A) the total energies (top left corner) and nonpolar contributions ($\Delta E_{vdw} + \Delta G_{SA}$) (lower right corner) for all residues in the simulations. (B) Correlation between total energies (top left corner) and nonpolar contributions (lower right corner) for the α6 and α7 residues. (C) Total energies of the α3 residues and those of the α6 and α7 residue. (D) Nonpolar contributions of the α3 residues and those of the α6 and α7 residues.

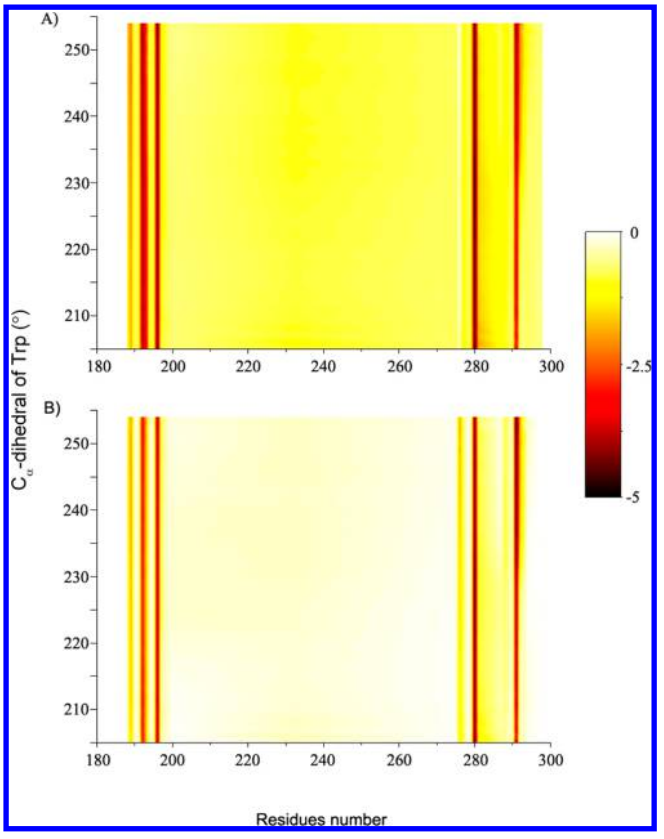

Figure 5. Visualization of the residue−BB3 interactions based on the MM/GBSA free energy decomposition analyses for all conformation groups. (A) Total binding free energies. (B) Nonpolar contributions ($\Delta E_{vdw} + \Delta G_{SA}$).

for the α3, α6, and α7 interaction network and the binding energy contributions of these key residues are highlighted in Figure 5 (detailed data of the key residues are summarized in Figure S2, Supporting Information), where the dark red color denotes high energy contribution and the light color represents low energy contribution.

The total binding free energies and nonpolar contributions of all residues for all conformation groups are illustrated in Figure 5A and B. After careful observations, we found that the important residues can be roughly categorized into three classes: (1) class I represented by the dark straight lines, (2) class II represented by the straight lines with gradual variation from red to yellow, and (3) class III represented by the straight lines with color changed from dark red to lighter red. To classify the important residues quantitatively, the difference of the total binding free energy for each residue between the 207° and the 251° conformation groups, the mean value of the total binding free energies of all conformation groups, and the change rate based on the mean value and the difference were calculated. The results for the important residues are summarized in Table 2. On the basis of the data shown in Table 2, the residues with the total binding free energy of the 247° group more negative than −2.0 kcal/mol, and the change rate lower than 25% are categorized into class I. The residues with the change rate higher than 25%, the total binding free energy of the 247° conformation group lower than −0.5 kcal/mol, and the absolute difference of the total binding free energies more positive than 0.5 kcal/mol are categorized into class II. The residues with the change rate higher than 25% and the total binding free energy of the 247° conformation group more negative than −0.5 kcal/mol or the absolute difference of the total binding free energies higher than 0.5 kcal/mol are categorized into class III.

The residues, including Leu192, Phe196, Phe280, and Trp281, belong to class I, and they can form strong and stable interactions with BB3 whether the WPD loop is open or closed. This fact suggests these residues are fundamental for the binding of BB3 in its binding site.

The residues, including Lys197, Glu276, Lys279, Val287, and Gln288, belong to class II, and their contributions show gradual variation with the decrease of the Trp179 C$_\alpha$-dihedral from 247° to 211°, suggesting that the interactions between BB3 and this class of residues decrease or increase gradually as the WPD loop swings from the open to the closed state. However, the energy contributions of these residues are not significant. Therefore, the residues in class II are not the most important residues for the allosteric inhibition mechanism.

As shown in Table 2, the residues, including Pro188, Ala189, Asn193, Ile281, Lys292, and Glu293, are the important residues in class III. The residues in class III can be further divided into two subclasses: class IIIa with Asn193 and Ile281 and class IIIb with Pro188, Ala189, Lys292, and Glu293. Two residues in class IIIa can form stronger interactions with BB3 at the closed state of the WPD loop, and their contributions become more favorable when the WPD loop changes from the open to the

dx.doi.org/10.1021/ci300526u | J. Chem. Inf. Model. 2013, 53, 1157−1167

Table 2. Change of Binding Free Energies for the Key Residues

class	residue	difference (kal/mol)	ΔG_{tot} of 247° group (kal/mol)	ΔG_{tot} of 211° group (kal/mol)	mean value (kal/mol)	relative change (%)
class IIIb	Pro188	0.51	−0.75 ± 0.13	−0.40 ± 0.11	−0.54	−94.44
	Ala189	0.42	−1.43 ± 0.18	−1.09 ± 0.14	−1.19	−35.29
	Lys292	1.29	−1.32 ± 0.21	0.01 ± 0.05	−0.57	−226.32
	Glu293	0.72	−0.64 ± 0.24	0.04 ± 0.06	−0.25	−288.00
class IIIa	Asn193	−0.62	−1.82 ± 0.35	−2.37 ± 0.27	−2.12	29.25
	Ile281	−0.24	−0.74 ± 0.19	−0.84 ± 0.16	−0.74	32.43
class II	Lys197	0.24	−0.43 ± 0.09	−0.25 ± 0.12	−0.35	−68.57
	Glu276	−0.10	0.43 ± 0.32	0.37 ± 0.26	0.40	−25.00
	Lys279	0.10	−0.28 ± 0.12	−0.23 ± 0.10	−0.24	−41.67
	Val287	−0.29	−0.10 ± 0.03	−0.28 ± 0.11	−0.26	111.54
	Gln288	0.22	−0.44 ± 0.09	−0.30 ± 0.09	−0.36	−61.11
class I	Leu192	0.34	−3.19 ± 0.26	−3.04 ± 0.27	−3.02	−11.26
	Phe196	0.09	−3.45 ± 0.22	−3.48 ± 0.16	−3.42	−2.63
	Phe280	−0.27	−3.73 ± 0.23	−3.63 ± 0.21	−3.73	7.24
	Trp291	0.33	−3.18 ± 0.27	−2.91 ± 0.39	−2.95	−11.12

closed state. In contrast, the residues in class IIIb can form more negative interactions with BB3 at the open state of the WPD loop, and therefore when the WPD loop changes from the open to the closed state the interactions between BB3 and the residues in class IIIb become much weaker. Thus, the residues in class IIIb are extremely important to determine the allosteric inhibition caused by the conformational change of the WPD loop.

The total binding free energy versus the value of the Trp179 C_α-dihedral in each conformation group for the residues in class IIIb is plotted in Figure 6. It can be observed that Lys292 is the

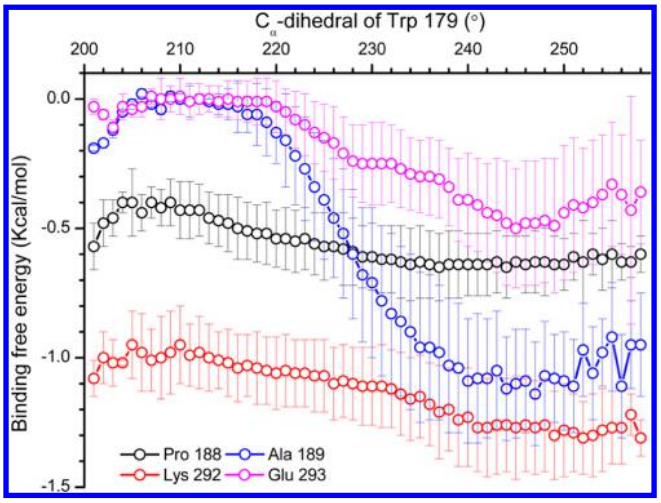

Figure 6. Change of total binding free energies of the four important residues in class IIIb.

most significant residue with the change rate up to −225.68%. The huge change rate suggests that the contribution of Lys292 for BB3 binding becomes much weaker as the WPD loop swings from the open to the closed conformation. The energy terms of Lys292 for all conformation groups are illustrated in Figure 7. It is clear that when the C_α-dihedral of Trp179 changes from 247° to 211°, the absolute values of ΔE_{vdw}, ΔE_{ele}, and ΔG_{SA} decrease and that of ΔG_{GB} increases. The most important energy term, ΔE_{vdw}, increases sharply from the 235° group to the 230° group.

3.4. Analysis of Movement of *α*7 Helix. The root-mean-square fluctuation (RMSF) is helpful to demonstrate the

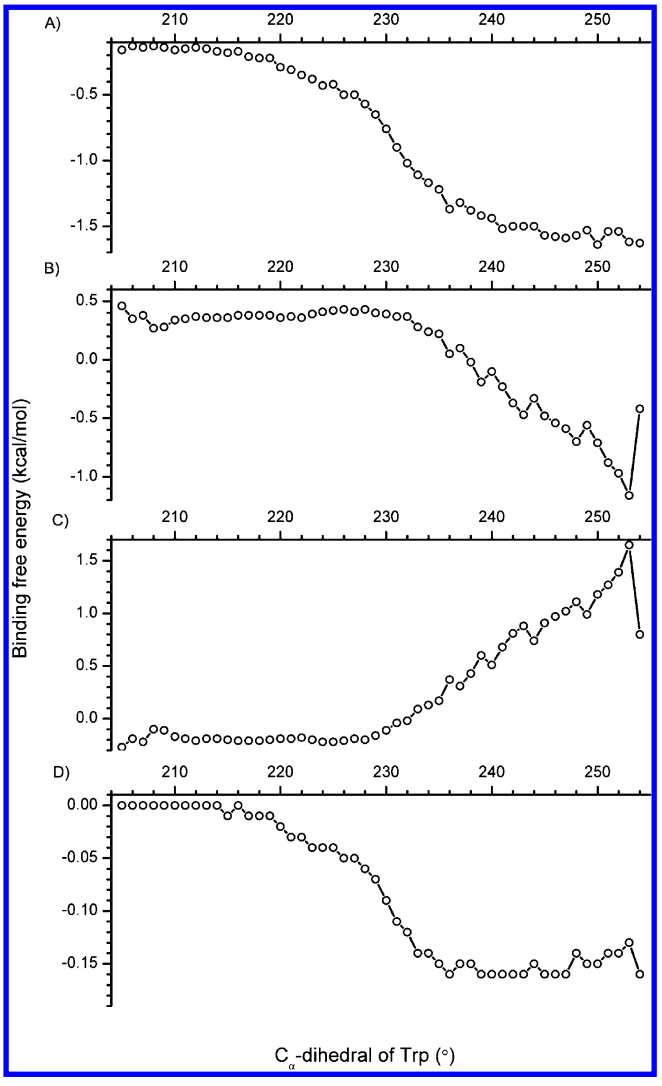

Figure 7. Change of the mean values of the (A) van der Waals energy term, (B) electrostatic term, (C) polar desolvation term, and (D) nonpolar desolvation term of Lys292 for all conformation groups.

fluctuations of residues with the conformational transition of the WPD loop. Herein, the RMSF profiles were calculated, and the differences of RMSF between the umbrella sampling MD

dx.doi.org/10.1021/ci300526u | J. Chem. Inf. Model. 2013, 53, 1157−1167

simulations and the equilibrium MD simulations are shown in Figure 8. Because of the energy perturbation by artificially

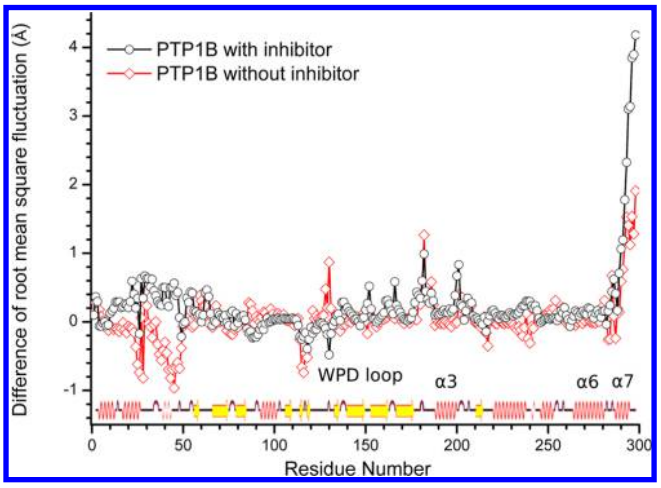

Figure 8. Difference of the root-mean-square fluctuations between the umbrella sampling MD simulations and the equilibrium MD simulations.

imposing harmonic biasing potential, the umbrella sampling MD trajectory shows higher mobility than that from the equilibrium MD simulations. As shown in Figure 8, the WPD loop is highly flexible in the umbrella sampling simulations. Furthermore, the α7 helix demonstrates higher mobility than the WPD loop abnormally in the complex. Considering the absence of the α7 helix in the crystal structures with the open WPD loop, we can infer that the α7 helix is unstable in the open WPD loop conformation, and the artificially constrained movement of the WPD loop with the allosteric inhibitor BB3 may lead to abnormal swing of the α7 helix.

The closest distances between the C_α atoms of the α7 helix and those of the α3 helix for all snapshots in each conformation group were measured, and the results are shown in Figure 9. Before comparing the trajectories of complex and protein without BB3, the lowest-energy conformers without the α3, α6, and α7 helix in the 247° and 211° groups of the protein trajectory were aligned based on the C_α atoms (Figure S3, Supporting Information). With the movement of the WPD loop from the open to the closed conformation, the closest distance of complex changes more obviously than that of PTP1B without inhibitor, suggesting that the inhibitor may makes the α7 helix move away from the α3 helix during the conformational change. Notably, the closest distance increases sharply when the Trp179 C_α-dihedral decreases from 235° to 230°. Furthermore, we found that the binding free energy contributions of Lys292 and Glu293 become more positive when the Trp179 C_α-dihedral decreases from 235° to 230°. The correlation coefficients between the closest distance and the energy contributions of Lys292 and Glu293 are 0.77 and 0.76, respectively, while the correlation coefficients for the 21 conformation groups with the Trp179 C_α-dihedral from 245° to 225° are 0.96 and 0.99, respectively, suggesting that when the α7 helix swings away from the α3 helix and the allosteric inhibitor the binding free energy contributions from the α7 residues become much more positive.

The lowest-energy conformers in the 247° and 211° groups were compared by aligning their C_α atoms between Glu1 to Asp298 except the WPD loop residues (Figure 10). The

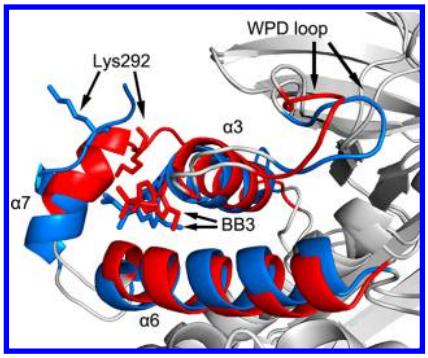

Figure 10. Comparison between the lowest energy structure of the typical open conformation group (red) and that of the typical closed conformation group (blue). The structures were aligned based on the coordinates of the C_α atoms.

difference of Lys292 between those two structures is highlighted. In comparison with the open state, the Lys292 and α7

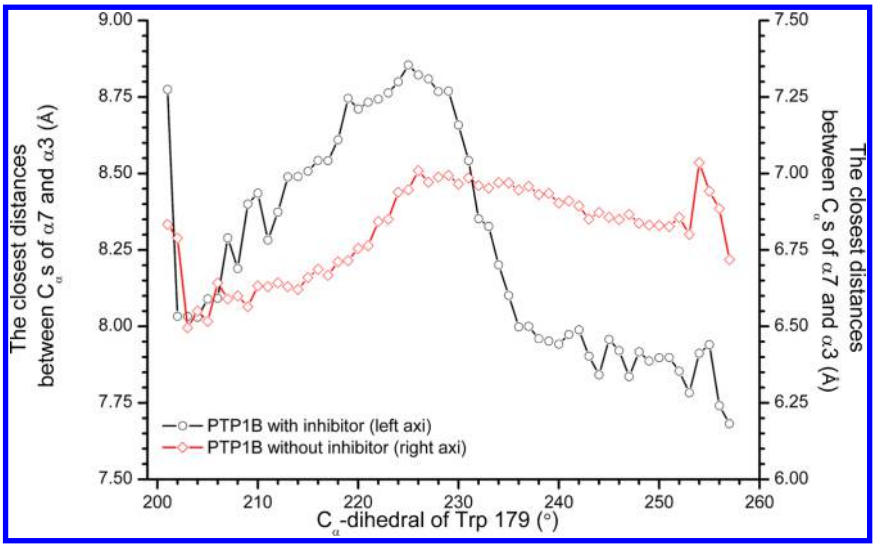

Figure 9. Closest distances between the C_α atoms of the α3 helix and those of the α7 helix for all conformation groups.

dx.doi.org/10.1021/ci300526u | J. Chem. Inf. Model. 2013, 53, 1157−1167

helix in the closed state move away from the binding site. Moreover, we notice that the terminal of the α3 helix is unwound in the closed state. This phenomenon may be explained by the two reasons. First, the unwounded part is the terminal of the whole structure, and it may undergo unwound due to the instability of the terminal. Second, the unwound of the α7 helix may be caused by the artificial harmonic biasing potential. The harmonic biasing potential forced the WDP loop to move from the open state to the closed state, which leads to the crash between BB3 and the α7 helix as we have discussed. Such crash will never happen without the artificial harmonic biasing potential but may lead to the unwound of the crashed part of the α7 helix. The movement of the WPD loop may be associated with the movement of α3, and this movement need a space near α6 and α7. If this space is occupied by an inhibitor, without additional energy provided by the artificial harmonic biasing potential of the umbrella sampling, the movement of the WPD loop and its associated movement will be hindered, and the mobility of the whole system will be confined. For all the crystal structures of the PTP proteins, PTP1B is the only member with the α7 helix structure,[61] and the allosteric inhibition mechanism demonstrates that the compound with strong interaction with the α7 residues especially Lys292 will result in highly selective PTP1B inhibitor.

4. CONCLUSIONS

In this study, the conformational transition of the WPD loop was studied by the umbrella sampling technique using the C_α-dihedral of Trp179 as the reaction coordinate supplemented with the MM/GBSA studies on the generated conformers. The binding free energy profile suggests that the complex of PTP1B and BB3 becomes more unstable when the WPD loop changes from the open to the closed state. Analysis of the binding free energy terms demonstrates that the allosteric inhibitor with more negative van der Waals contribution cannot only exhibit stronger binding affinity but also hinder the swing of the WPD loop more effectively.

on the basis of the residue inhibitor interaction spectra, the key residues for determining the mechanism of allosteric inhibition were clearly determined. The correlation analysis of the residues located in different regions suggests that most of the important residues are located in the α3, α6, and α7 helices, and the variations of the energy contributions of these important residues are correlated between the three regions. Moreover, the important residues were categorized into three classes. (1) Class I has the residues with strong and stable interactions with the inhibitor. (2) Class II has the residues whose energy contributions change slightly. (3) Class III has the key residues, which show significantly changeable energy contributions when the WPD loop changes from the open to the closed state. Therefore, it was effective to enhance the allosteric inhibition capability by improving the van der Waals interactions between inhibitor and these residues in class IIIb.

Among the residues in class IIIb, Lys292 was found to be the most special one because its binding energy changes dramatically. Furthermore, the RMSF analysis of the umbrella sampling and the structural analysis demonstrate that the α7 helix is highly mobile during the simulations and moves away from the binding site. The results clearly show that the α7 helix moves with the swing of the WPD loop during the simulations, leading to the change of the van der Waals interaction of BB3 with the binding site and the unfavorable binding affinity. Therefore, it can be concluded that the improvement of the van der Waals interaction of BB3 with Lys292 will be helpful to improve the binding affinity and the selectivity of allosteric PTP1B inhibitors. Our study demonstrates that umbrella sampling technique supplemented with the MM/GBSA free energy prediction is a feasible way to elucidate the allosteric inhibition mechanism.

■ ASSOCIATED CONTENT

Supporting Information

Part S1: Details of the statistical significance test of correlation and other analyses. Part S2: Effect of the length of the umbrella sampling simulations. Table S1: *T*-values of the paired *t*-test for each residue pair of the class II and class IIIb residues. Figure S1: Relationships between Trp179 C_α-dihedral and the other four conformational parameters. Figure S2: Binding free energy contributions of the important residues during the conformational change (kcal/mol). Figure S3: Structural alignment of the lowest-energy conformers without the α3, α6, and α7 helices in the 247° and 211° groups based on the C_α atoms. Figure S4: MM/GBSA binding free energies of the conformation groups. Figure S5: Change of the total binding free energies of the four important residues in class IIIb. This material is available free of charge via the Internet at http://pubs.acs.org.

■ AUTHOR INFORMATION

Corresponding Author

*E-mail: jmj@ucas.ac.cn (M.-J.J.); tingjunhou@hotmail.com or tingjunhou@zju.edu.cn (T.-J.H.). Tel.: +86 10 88256326 (M.-J.J.); +86 512 65882039 (T.-J.H.). Fax: +86 10 88256093 (M.-J.J.).

Notes

The authors declare no competing financial interest.

■ ACKNOWLEDGMENTS

The project was supported by the National Science Foundation of China (21173264 and 21173156), the Foundation of Knowledge Innovative Engineering of Chinese Academy of Sciences (ZNWH-2011-011) and Presidential Fund of UCAS (Y25101BY00). Thanks to Professor San-guo Zhang (School of Mathematics, UCAS) for his helpful discussions on the statistical significance test.

■ REFERENCES

(1) Huang, Z.; Zhu, L.; Cao, Y.; Wu, G.; Liu, X.; Chen, Y.; Wang, Q.; Shi, T.; Zhao, Y.; Wang, Y. ASD: A comprehensive database of allosteric proteins and modulators. *Nucleic Acids Res.* **2011**, *39*, D663−D669.

(2) Stadtman, E. R. *Allosteric Regulation of Enzyme Activity*, 1966/01/01 ed.; Intescience Publishers: New York, 1966; Vol. *28*, pp 41−154.

(3) VanWart, A. T.; Eargle, J.; Schulten, Z.; Amaro, R. E. Exploring residue component contributions to dynamical network models of allostery. *J. Chem. Theory Comput.* **2012**, *8*, 2949−2961.

(4) Reynolds, K. A.; McLaughlin, R. N.; Ranganathan, R. Hot spots for allosteric regulation on protein surfaces. *Cell* **2011**, *147*, 1564−1575.

(5) Byon, J. C. H.; Kusari, A. B.; Kusari, J. Protein-tyrosine phosphatase-1B acts as a negative regulator of insulin signal transduction. *Mol. Cell. Biochem.* **1998**, *182*, 101−108.

(6) Tiganis, T. PTP1B and TCPTP: Nonredundant phosphatases in insulin signaling and glucose homeostasis. *FEBS J.* **2012**, *280*, 445−458.

(7) Zhang, S.; Zhang, Z. Y. PTP1B as a drug target: Recent developments in PTP1B inhibitor discovery. *Drug Discovery Today* **2007**, *12*, 373−381.
(8) Zhang, Z. Y.; Lee, S. Y. PTP1B inhibitors as potential therapeutics in the treatment of type 2 diabetes and obesity. *Expert Opin. Invest. Drugs* **2003**, *12*, 223−233.
(9) Cheng, A.; Uetani, N.; Simoncic, P. D.; Chaubey, V. P.; Lee-Loy, A.; McGlade, C. J.; Kennedy, B. P.; Tremblay, M. L. Attenuation of leptin action and regulation of obesity by protein tyrosine phosphatase 1B. *Dev. Cell* **2002**, *2*, 497−503.
(10) Heneberg, P. Use of protein tyrosine phosphatase inhibitors as promising targeted therapeutic drugs. *Curr. Med. Chem.* **2009**, *16*, 706−733.
(11) Stuible, M.; Doody, K. M.; Tremblay, M. L. PTP1B and TC-PTP: Regulators of transformation and tumorigenesis. *Cancer Metastasis Rev.* **2008**, *27*, 215−30.
(12) Kamerlin, S. C. L.; Rucker, R.; Boresch, S. A targeted molecular dynamics study of WPD loop movement in PTP1B. *Biochem. Biophys. Res. Commun.* **2006**, *345*, 1161−1166.
(13) DeLano, W. L. *PyMOL Molecular Graphics System*, 2002. http://pymol.sourceforge.net/overview/index.htm (accessed May 6, 2013).
(14) Jia, Z.; Barford, D.; Flint, A. J.; Tonks, N. K. Structural basis for phosphotyrosine peptide recognition by protein tyrosine phosphatase 1B. *Science* **1995**, *268*, 1754−1758.
(15) Wiesmann, C.; Barr, K. J.; Kung, J.; Zhu, J.; Erlanson, D. A.; Shen, W.; Fahr, B. J.; Zhong, M.; Taylor, L.; Randal, M. Allosteric inhibition of protein tyrosine phosphatase 1B. *Nat. Struct. Mol. Biol.* **2004**, *11*, 730−737.
(16) Khajehpour, M.; Wu, L.; Liu, S.; Zhadin, N.; Zhang, Z. Y.; Callender, R. Loop dynamics and ligand binding kinetics in the reaction catalyzed by the Yersinia protein tyrosine phosphatase. *Biochemistry* **2007**, *46*, 4370−4378.
(17) Juszczak, L. J.; Zhang, Z. Y.; Wu, L.; Gottfried, D. S.; Eads, D. D. Rapid loop dynamics of Yersinia protein tyrosine phosphatases. *Biochemistry* **1997**, *36*, 2227−2236.
(18) Sarmiento, M.; Zhao, Y.; Gordon, S. J.; Zhang, Z. Y. Molecular basis for substrate specificity of protein-tyrosine phosphatase 1B. *J. Biol. Chem.* **1998**, *273*, 26368−26374.
(19) Schlick, T. Molecular dynamics-based approaches for enhanced sampling of long-time, large-scale conformational changes in biomolecules. *F1000 Biol. Rep.* **2009**, *1*, 51.
(20) Roux, B. The calculation of the potential of mean force using computer-simulations. *Comput. Phys. Commun.* **1995**, *91*, 275−282.
(21) Torrie, G.; Valleau, J. Nonphysical sampling distributions in Monte Carlo free-energy estimation: Umbrella sampling. *J. Comput. Phys.* **1977**, *23*, 187−199.
(22) Homeyer, N.; Gohlke, H. Free energy calculations by the molecular mechanics Poisson−Boltzmann surface area method. *Mol. Inf.* **2012**, *31*, 114−122.
(23) Kollman, P. A.; Massova, I.; Reyes, C.; Kuhn, B.; Huo, S. H.; Chong, L.; Lee, M.; Lee, T.; Duan, Y.; Wang, W.; Donini, O.; Cieplak, P.; Srinivasan, J.; Case, D. A.; Cheatham, T. E. Calculating structures and free energies of complex molecules: Combining molecular mechanics and continuum models. *Acc. Chem. Res.* **2000**, *33*, 889−897.
(24) Wang, J. M.; Hou, T. J.; Xu, X. J. Recent advances in free energy calculations with a combination of molecular mechanics and continuum models. *Curr. Comput.-Aided Drug Des.* **2006**, *2*, 287−306.
(25) Gohlke, H.; Kiel, C.; Case, D. A. Insights into protein−protein binding by binding free energy calculation and free energy decomposition for the Ras−Raf and Ras−RalGDS complexes. *J. Mol. Biol.* **2003**, *330*, 891−913.
(26) Hou, T. J.; Xu, Z.; Zhang, W.; McLaughlin, W. A.; Case, D. A.; Xu, Y.; Wang, W. Characterization of domain−peptide interaction Interface: A generic structure-based model to decipher the binding specificity of SH3 domains. *Mol. Cell. Proteomics* **2009**, *8*, 639−649.
(27) Hou, T. J.; Zhang, W.; Case, D. A.; Wang, W. Characterization of domain−peptide interaction interface: A case study on the amphiphysin-1 SH3 domain. *J. Mol. Biol.* **2008**, *376*, 1201−1214.
(28) *Sybyl*, version 7.1; Tripos: St. Louis, MO, 2005.
(29) Frisch, M. J.; Trucks, G. W.; Schlegel, H. B.; Scuseria, G. E.; Robb, M. A.; Cheeseman, J. R.; Montgomery, J. A., Jr.; Vreven, T.; Kudin, K. N.; Burant, J. C.; Millam, J. M.; Iyengar, S. S.; Tomasi, J.; Barone, V.; Mennucci, B.; Cossi, M.; Scalmani, G.; Rega, N.; Petersson, G. A.; Nakatsuji, H.; Hada, M.; Ehara, M.; Toyota, K.; Fukuda, R.; Hasegawa, J.; Ishida, M.; Nakajima, T.; Honda, Y.; Kitao, O.; Nakai, H.; Klene, M.; Li, X.; Knox, J. E.; Hratchian, H. P.; Cross, J. B.; Bakken, V.; Adamo, C.; Jaramillo, J.; Gomperts, R.; Stratmann, R. E.; Yazyev, O.; Austin, A. J.; Cammi, R.; Pomelli, C.; Ochterski, J. W.; Ayala, P. Y.; Morokuma, K.; Voth, G. A.; Salvador, P.; Dannenberg, J. J.; Zakrzewski, V. G.; Dapprich, S.; Daniels, A. D.; Strain, M. C.; Farkas, O.; Malick, D. K.; Rabuck, A. D.; Raghavachari, K.; Foresman, J. B.; Ortiz, J. V.; Cui, Q.; Baboul, A. G.; Clifford, S.; Cioslowski, J.; Stefanov, B. B.; Liu, G.; Liashenko, A.; Piskorz, P.; Komaromi, I.; Martin, R. L.; Fox, D. J.; Keith, T.; Al-Laham, M. A.; Peng, C. Y.; Nanayakkara, A.; Challacombe, M.; Gill, P. M. W.; Johnson, B.; Chen, W.; Wong, M. W.; Gonzalez, C.; Pople, J. A. *Gaussian 03*, revision C.02 ; Gaussian, Inc.: Wallingford, CT, 2004.
(30) Bayly, C. I.; Cieplak, P.; Cornell, W.; Kollman, P. A. A well-behaved electrostatic potential based method using charge restraints for deriving atomic charges: the RESP model. *J. Phys. Chem.* **1993**, *97*, 10269−10280.
(31) Wang, J.; Wang, W.; Kollman, P. A.; Case, D. A. Automatic atom type and bond type perception in molecular mechanical calculations. *J. Mol. Graphics Modell.* **2006**, *25*, 247−260.
(32) Duan, Y.; Wu, C.; Chowdhury, S.; Lee, M. C.; Xiong, G.; Zhang, W.; Yang, R.; Cieplak, P.; Luo, R.; Lee, T. A point-harge force field for molecular mechanics simulations of proteins based on condensed-phase quantum mechanical calculations. *J. Comput. Chem.* **2003**, *24*, 1999−2012.
(33) Wang, J. M.; Wolf, R. M.; Caldwell, J. W.; Kollman, P. A.; Case, D. A. Development and testing of a general amber force field. *J. Comput. Chem.* **2004**, *25*, 1157−1174.
(34) Jorgensen, W. L.; Chandrasekhar, J.; Madura, J. D.; Impey, R. W.; Klein, M. L. Comparison of simple potential functions for simulating liquid water. *J. Chem. Phys.* **1983**, *79*, 926−935.
(35) Case, D. A.; Cheatham, T. E.; Darden, T.; Gohlke, H.; Luo, R.; Merz, K. M.; Onufriev, A.; Simmerling, C.; Wang, B.; Woods, R. J. The Amber biomolecular simulation programs. *J. Comput. Chem.* **2005**, *26*, 1668−1688.
(36) Harvey, S. C.; Tan, R. K. Z.; Cheatham, T. E., III The flying ice cube: Velocity rescaling in molecular dynamics leads to violation of energy equipartition. *J. Comput. Chem.* **1998**, *19*, 726−740.
(37) Ryckaert, J. P.; Ciccotti, G.; Berendsen, H. J. C. Numerical integration of the cartesian equations of motion of a system with constraints: molecular dynamics of n-alkanes. *J. Comput. Phys.* **1977**, *23*, 327−341.
(38) Darden, T.; York, D.; Pedersen, L. Particle mesh Ewald: An $N\cdot\log(N)$ method for Ewald sums in large systems. *J. Comput. Phys.* **1993**, *98*, 10089−10092.
(39) Kamerlin, S. C. L.; Rucker, R.; Boresch, S. A molecular dynamics study of WPD-loop flexibility in PTP1B. *Biochem. Biophys. Res. Commun.* **2007**, *356*, 1011−1016.
(40) Genheden, S.; Ryde, U. How to obtain statistically converged MM/GBSA results. *J. Comput. Chem.* **2010**, *31*, 837−846.
(41) Genheden, S.; Ryde, U. Comparison of the efficiency of the LIE and MM/GBSA methods to calculate ligand-binding energies. *J. Chem. Theory Comput.* **2011**, *7*, 3768−3778.
(42) Gohlke, H.; Case, D. A. Converging free energy estimates: MM-PB (GB) SA studies on the protein−protein complex Ras−Raf. *J. Comput. Chem.* **2004**, *25*, 238−250.
(43) Hou, T.; Yu, R. Molecular dynamics and free energy studies on the wild-type and double mutant HIV-1 protease complexed with amprenavir and two amprenavir-related inhibitors: mechanism for binding and drug resistance. *J. Med. Chem.* **2007**, *50*, 1177−1188.
(44) Hou, T. J.; Wang, J. M.; Li, Y. Y.; Wang, W. Assessing the performance of the molecular mechanics/Poisson Boltzmann surface area and molecular mechanics/generalized Born surface area methods.

II. The accuracy of ranking poses generated from docking. *J. Comput. Chem.* **2011**, *32*, 866−77.
(45) Hou, T. J.; Wang, J. M.; Li, Y. Y.; Wang, W. Assessing the performance of the MM/PBSA and MM/GBSA methods. 1. The accuracy of binding free energy calculations based on molecular dynamics simulations. *J. Chem. Inf. Mol. Model.* **2011**, *51*, 69−82.
(46) Hou, T. J.; Zhu, L. L.; Chen, L. R.; Xu, X. J. Mapping the binding site of a large set of quinazoline type EGF-R inhibitors using molecular field analyses and molecular docking studies. *J. Chem. Inf. Comput. Sci.* **2003**, *43*, 273−287.
(47) Huo, S.; Massova, I.; Kollman, P. A. Computational alanine scanning of the 1:1 human growth hormone−receptor complex. *J. Comput. Chem.* **2002**, *23*, 15−27.
(48) Huo, S.; Wang, J.; Cieplak, P.; Kollman, P. A.; Kuntz, I. D. Molecular dynamics and free energy analyses of cathepsin D-inhibitor interactions: Insight into structure-based ligand design. *J. Comput. Chem.* **2002**, *45*, 1412−1419.
(49) Kuhn, B.; Kollman, P. A. Binding of a diverse set of ligands to avidin and streptavidin: An accurate quantitative prediction of their relative affinities by a combination of molecular mechanics and continuum solvent models. *J. Med. Chem.* **2000**, *43*, 3786−3791.
(50) Liu, H.; Yao, X. Molecular basis of the interaction for an essential subunit PA-PB1 in influenza virus RNA polymerase: Insights from molecular dynamics simulation and free energy calculation. *Mol. Pharmaceut.* **2009**, *7*, 75−85.
(51) Liu, H.; Yao, X.; Wang, C.; Han, J. In silico identification of the potential drug resistance sites over 2009 influenza A (H1N1) virus neuraminidase. *Mol. Pharmaceut.* **2010**, *7*, 894−904.
(52) Weis, A.; Katebzadeh, K.; Soderhjelm, P.; Nilsson, I.; Ryde, U. Ligand affinities predicted with the MM/PBSA method: Dependence on the simulation method and the force field. *J. Med. Chem.* **2006**, *49*, 6596−6606.
(53) Xue, W.; Pan, D.; Yang, Y.; Liu, H.; Yao, X. Molecular modeling study on the resistance mechanism of HCV NS3/4A serine protease mutants R155K, A156V and D168A to TMC435. *Antiviral Res.* **2012**, *93*, 126−137.
(54) Li, L.; Li, Y.; Zhang, L.; Hou, T. Theoretical studies on the susceptibility of oseltamivir against variants of 2009 A/H1N1 influenza neuraminidase. *J. Chem. Inf. Mol. Model.* **2012**, *52*, 2715−2729.
(55) Tsui, V.; Case, D. A. Theory and applications of the generalized Born solvation model in macromolecular simulations. *Biopolymers* **2001**, *56*, 275−291.
(56) Weiser, J.; Shenkin, P. S.; Still, W. C. Approximate atomic surfaces from linear combinations of pairwise overlaps (LCPO). *J. Comput. Chem.* **1999**, *20*, 217−230.
(57) Hou, T.; Zhang, W.; Wang, J.; Wang, W. Predicting drug resistance of the HIV-1 protease using molecular interaction energy components. *Proteins: Struct., Funct., Bioinf.* **2009**, *74*, 837−846.
(58) Hou, T. J.; Li, N.; Li, Y. Y.; Wang, W. Characterization of domain-peptide interaction interface: Prediction of SH3 domain-mediated protein−protein interaction network in yeast by generic structure-based models. *J. Proteome Res.* **2012**, *11*, 2982−2995.
(59) Xu, Z.; Hou, T.; Li, N.; Xu, Y.; Wang, W. Proteome-wide detection of Abl1 SH3-binding peptides by integrating computational prediction and peptide microarray. *Mol. Cell. Proteomics* **2012**, *11*, O111.010389.
(60) *Scilab*, version 5.4.1; Scilab Enterprises: Versailles, France, 2012.
(61) Tabernero, L.; Aricescu, A. R.; Jones, E. Y.; Szedlacsek, S. E. Protein tyrosine phosphatases: Structure−function relationships. *FEBS J.* **2008**, *275*, 867−882.